metals

MDPI

Article

Effects of Vacancy Defects on Electrical and Optical Properties of ZnO/WSe_2 Heterostructure: First-Principles Study

Xi Yong [1], Ao Wang [1], Lichuan Deng [2], Xiaolong Zhou [2,*] and Jintao Li [2,*]

[1] Research Institute of Special Steels, Central Iron and Steel Research Institute, Beijing 100081, China
[2] Faculty of Materials Science and Engineering, Kunming University of Science and Technology, Kunming 650500, China
* Correspondence: kmzxlong@163.com (X.Z.); kmust502@163.com (J.L.)

Abstract: In this work, based on the first principles calculation of density functional theory (DFT), we studied the band structure changes of monolayer ZnO and ZnO/WSe_2 before and after vacancy generation, and systematically studied the vacancy formation energy, band structure, density of states, electronic density difference and optical properties of ZnO/WSe_2 heterostructure before and after vacancy generation. The results show that the band structures of ZnO, WSe_2, and ZnO/WSe_2 heterostructure are changed after the formation of Zn, O, W, and Se vacancies. The bandgap of the ZnO/WSe_2 heterostructure can be effectively controlled, the transition from direct to indirect bandgap semiconductor will occur, and the heterostructure will show metallic properties. The optical properties of heterostructure have also changed significantly, and the absorption capacity of heterostructure to infrared light has been greatly increased with red shift and blue shift respectively. The generation of vacancy changes the electrical and optical properties of ZnO/WSe_2 heterostructure, which provides a feasible strategy for adjusting the photoelectric properties of two-dimensional optoelectronic nano devices and has good potential and broad application prospects.

Keywords: first-principles; ZnO/WSe_2 heterostructure; vacancy; electrical properties; optical properties

check for updates

Citation: Yong, X.; Wang, A.; Deng, L.; Zhou, X.; Li, J. Effects of Vacancy Defects on Electrical and Optical Properties of ZnO/WSe_2 Heterostructure: First-Principles Study. *Metals* **2022**, *12*, 1975. https://doi.org/10.3390/met12111975

Academic Editors: Jiro Kitagawa and Jeff Th. M. De Hosson

Received: 17 October 2022
Accepted: 16 November 2022
Published: 18 November 2022

1. Introduction

In recent years, the shortage of fossil fuels and environmental degradation have forced the search for a clean, renewable fuel, and the conversion of visible light into hydrogen fuel is an advanced technology with great potential for application [1,2]. In 1972, Fujishima and Honda first used TiO_2 for water separation [3]. Two-dimensional nano-materials such as germanium, graphene, and transition metal-sulphur compounds, are widely used in the study of optoelectronic materials [4,5] and photocatalytic materials [6–8] because of their unique physical properties. Semiconductors are used in a wide range of applications, such as various electronic devices, photodetectors devices [9] and photovoltaic cells [10–12].

In recent decades, researchers have extensively explored the properties of semiconductors. Semiconductors doped with magnetic impurities, which are referred to as dilute magnetic semiconductors, have been developed toward spintronic applications [13,14]. These technologies usually rely on heterostructures fabricated under precisely controlled conditions [15]. Lattice defects have an important effect on the performance of devices and even play a decisive role [16–18]. Therefore, lattice defects play an important role in material properties or device properties [19]. For example, Qin et al. created vacancy defects in the $ZnIn_2S_4/g\text{-}C_3N_4$ heterojunction by calcination-solvothermal method, which greatly improved the photocatalytic performance of the $ZnIn_2S_4/g\text{-}C_3N_4$ heterojunction [20]. However, it is difficult to obtain lattice defects through experiments at the atomic and electronic levels. The calculation method is a supplement to the experimental research and provides detailed preliminary data for the experiment [21]. Therefore, using quantum mechanics or first principles to calculate the performance changes caused by lattice defects is a hot spot [22,23].

In this work, based on the first principles calculation of density functional theory (DFT), we studied the band structure changes of monolayer ZnO and WSe_2 before and after vacancy generation, and systematically studied the vacancy formation energy, band structure, density of states, electronic density difference and optical properties of ZnO/WSe_2 heterostructure before and after vacancy generation.

2. Computational Methods

In this study, we use first-principles density functional theory (DFT) [24] to study the properties of ZnO/WSe_2 heterostructure. The process is implemented by Cambridge Studio Total Energy Package (CASTEP) code [25] from Materials Studio. In order to ensure the accuracy and reliability of the calculation, we first conduct the convergence test of ZnO and WSe_2. Then, according to the comparison of the generalized gradient approximation (GGA) with Perdew-Burke-Ernzerhof (PBE) [26] and Heyd–Scuseria–Ernzerhos hybrid functional (HSE06) [27] in Fafei Hu [28,29], for ZnO/WSe_2 heterostructure, the bandgap calculated by HSE06 is larger. Our main research is the effect of different vacancy defects on the ZnO/WSe_2 heterostructure. Therefore, we choose the GGA-PBE exchange-correlation functional to describe the exchange-correlation interaction [30–32] under the premise of considering the calculation accuracy and calculation efficiency at the same time. We use the TS method for DFT + D correction to modify and correct the accuracy of the standard GGA-PBE function for the system, because the standard PBE function cannot well describe the vdW interaction. The K point of $6 \times 6 \times 1$ and the plane-wave kinetic energy cutoff of 440 eV are set for the geometry optimization. The Broyden-Fletcher-Goldfarb-Shanno(BFGS) [33] minimize-er was used to optimize the configured geometry to relax the crystal structure and atomic coordinates. The self-consistent convergence accuracy is set to 10^{-5} eV per atom, and the convergence criterion for the atomic force is 0.03 eV/Å. Considering that the w element is heavy, spin orbit interaction is used. The vacuum layer was set as 14 Å to minimize the interlayer interaction between periodic layers.

The formula of formation energy E_f for the vacancy in monolayer ZnO, WSe_2, and ZnO/WSe_2 heterostructure can be expressed as [34,35]:

$$E_f = E_{defect}(X) - E_{perfect} + \mu_0(X) \tag{1}$$

where $E_{defect}(X)$ is the total energy of structure containing defective atom X, $E_{perfect}$ is the total energy of perfect structure and $\mu_0(X)$ correspond to the chemical potentials of X atom.

In order to evaluate the stability of ZnO/WSe_2 heterostructure, according to the definition of binding energy (E_b) [36]:

$$E_b = E_{ZnO/WSe_2} - E_{ZnO} - E_{WSe_2} \tag{2}$$

where E_{ZnO/WSe_2}, E_{ZnO} and E_{WSe_2} are the total energy of ZnO/WSe_2 heterostructure, a monolayer of ZnO and WSe_2, respectively.

Based on the frequency-dependent dielectric function, the optical absorption coefficient $\alpha(\omega)$ can be calculated by the following formula [37]:

$$\alpha(\omega) = \sqrt{2}\omega\left[\sqrt{\varepsilon_1^2(\omega) + \varepsilon_2^2(\omega)} - \varepsilon_1(\omega)\right]^{\frac{1}{2}} \tag{3}$$

where, ε_1 and ε_2 are the real and imaginary parts of the dielectric function, respectively.

3. Results and Discussion

3.1. Structure and Stability

A bulk model of ZnO and WSe_2 (Zinc blende Structure) was first established, then single molecule models of ZnO (001) and WSe_2 (001) were obtained after optimization according to the above parameters, and finally a ZnO/WSe_2 heterojunction model was constructed. The possible vacancy positions of monolayer ZnO, WSe_2 and ZnO/WSe_2 heterostructure are shown in Figure 1. After optimization, the surface thickness of ZnO

is 0.635 Å, the surface thickness of WSe_2 is 1.68 Å, and the lattice constants of ZnO and WSe_2 are 6.410 Å and 6.651 Å, respectively. The calculated lattice mismatch is 3.7% which is less than 5%, so it is possible to build heterostructures of WSe_2 and ZnO without inducing structural defects. In order to evaluate the stability of the ZnO/WSe_2 heterostructure, the binding energy (E_b) of the ZnO/WSe_2 heterostructure is −1.276 eV according to Formula (2). It shows that the ZnO/WSe_2 heterostructure can exist stably. According to Formula (1), the formation energy E_f for the vacancy of ZnO−V_O and ZnO−V_{Zn}, WSe_2−V_W and WSe_2−V_{Se}, ZnO/WSe_2−V_{Zn}, ZnO/WSe_2−V_O, ZnO/WSe_2−V_W, and ZnO/WSe_2−V_{Se} heterostructure are calculated respectively, and the results are shown in Table 1. According to the calculation results, except for E_f (ZnO/WSe_2−V_{Zn}), the rest E_f is positive, which indicates that all the structures can exist stably except ZnO/WSe_2−V_{Zn} heterostructure. The formation energy E_f for vacancy of ZnO/WSe_2−V_{Se} is the smallest, which indicates that the structure of ZnO/WSe_2−V_{Se} is the easiest to form. For ZnO/WSe_2−V_{Zn}, we also hope to study its structure and properties, find out the reasons for its structural instability, and compare and analyze it with other similar structures.

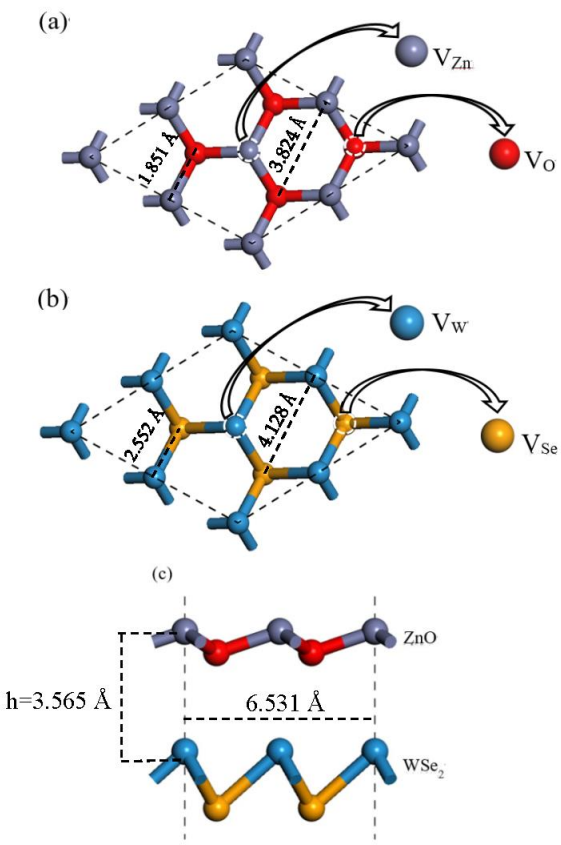

Figure 1. (**a**) Schematic diagram of possible vacancies in monolayer ZnO (**b**) Schematic diagram of possible vacancies in monolayer WSe_2 (**c**) Schematic diagram of possible vacancies in heterojunction ZnO/WSe_2. V_{Zn}, V_O, V_W, and V_{Se} represent the possible vacancy positions of Zn, O, W and Se.

3.2. Electronic Properties

The energy band structures of monolayer ZnO, ZnO−V_O and ZnO−V_{Zn} are shown in Figure 2. By comparison, it can be seen from the figure that monolayer ZnO is a semiconductor with a direct band gap of 1.639 eV, and the results are similar to 1.69 eV in the literature [28]. When Zn vacancies are generated, it is interesting that ZnO transforms from semiconductor to metal, showing obvious metallic properties. When the O vacancy is generated, the monolayer ZnO remains a direct bandgap semiconductor, but the bandgap increases to 2.156 eV.

Table 1. The formation energy Ef (eV) for the vacancy in monolayer ZnO, WSe_2 and ZnO/WSe_2 heterostructure. V_{Zn} means Zn vacancy is generated; similarly, V_O, V_W and V_{Se} mean O, W and Se vacancy are generated.

Vacancy \ Structure	ZnO	WSe_2	ZnO/WSe_2
V_{Zn}	6.44		−2.56
V_O	8.13		7.90
V_W		7.66	10.59
V_{Se}		3.40	0.40

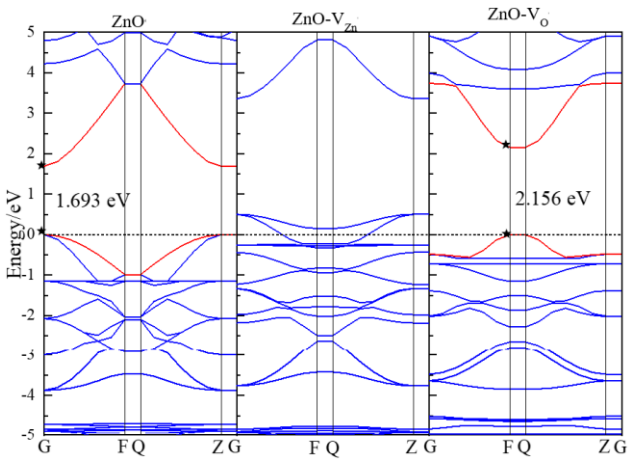

Figure 2. The band structure of ZnO, $ZnO-V_O$ and $ZnO-V_{Zn}$. Fermi levels are represented by dashed lines, and the conduction band minimum (CBM) and valence band maximum (VBM) are marked by black stars.

The band structures of monolayer WSe_2, $WSe_2-V_{W,}$ and WSe_2-V_{Se} are shown in Figure 3. By comparison, it can be seen that the monolayer WSe_2 is a semiconductor with a direct bandgap of 1.322 eV, and the results are similar to 1.92 in the literature [29]. When W and Se vacancies are generated, the transition from direct to indirect bandgap semiconductors is caused, and the indirect bandgaps are 1.427 eV and 1.363 eV, respectively. The valence band of WSe_2-V_{Se} is more densely distributed, while WSe_2-V_W produces an empty band of about 1 eV in the valence band.

The band structure and density of states (DOS) of ZnO/WSe_2 heterostructure, ZnO/WSe_2-V_{Zn}, ZnO/WSe_2-V_O, ZnO/WSe_2-V_W, and ZnO/WSe_2-V_{Se} are shown in Figure 4 and Figure 5, respectively. It can be seen from Figure 4 that ZnO/WSe_2 heterostructure is a semiconductor with a direct bandgap of 1.363 eV, and the results are also similar to those in the literature [28]. When the Zn vacancy is generated, the direct bandgap of ZnO/WSe_2 heterostructure increases to 1.504 eV; when the O vacancy is generated, the valence band crosses the Fermi level, and the transition from semiconductor to metal takes place, showing obvious metal behavior, which is opposite to that of $ZnO-V_O$ and $ZnO-V_{Zn}$ in monolayer ZnO. When W and Se vacancies are generated, the transition from direct to indirect bandgap semiconductors occurs, and the indirect bandgap is 1.168 eV and 1.729 eV, respectively. In addition, all the vacancies except ZnO/WSe_2-V_O will cause the unoccupied state above the Fermi level, that is, the gap in the conduction band near the Fermi level. The local magnetic moment appears and is reflected by the spin polarization in the corresponding band structure due to a vacancy in the heterostructure.

It can be seen from Figure 5a–e that the total density of states (DOS) of the heterostructure decreases after the vacancy is generated. That is because the total DOS of the heterostructure decreases after the loss of an atom. The density of states of ZnO/WSe_2-V_O heterostructure is beyond the Fermi level, showing obvious metallic properties. Generally speaking, for the same structure, the lower the density of states at the Fermi level, the more

stable the structure is [38]. Comparing with Figure 5b,d,e, it can be seen that the DOS at the Fermi level of ZnO/WSe_2-V_{Zn} is the highest, which indicates that its structure is unstable; The lowest DOS at the Fermi level of ZnO/WSe_2-V_{Se} indicates that it is more stable, Which is the same as the conclusion obtained from the calculation of vacancy formation energy in Section 3.1.

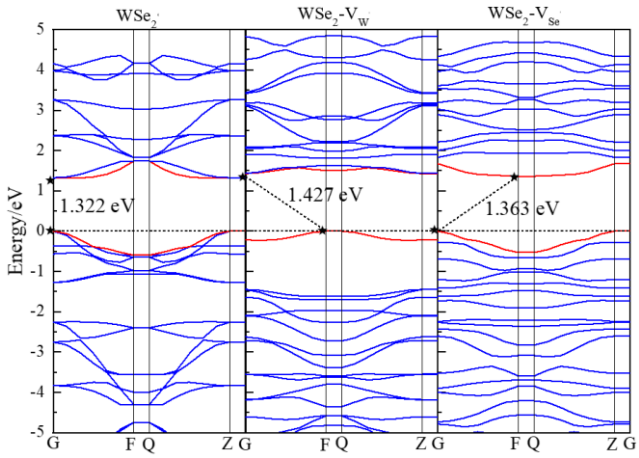

Figure 3. The band structure of WSe_2, WSe_2-V_W, and WSe_2-V_{Se}. Fermi levels are represented by dashed lines, and the CBM and VBM are marked by black stars.

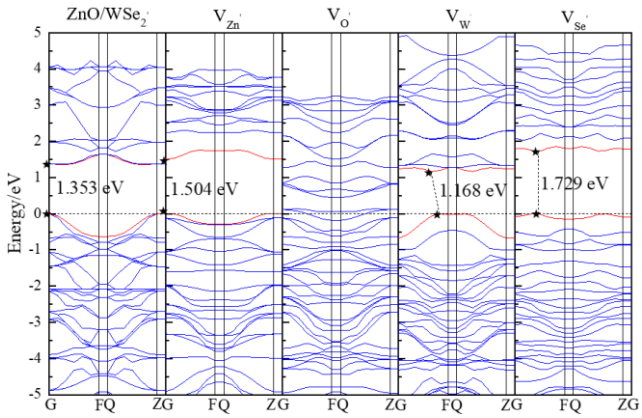

Figure 4. The band structure of ZnO/WSe_2 heterostructure, ZnO/WSe_2-V_{Zn}, ZnO/WSe_2-V_O, ZnO/WSe_2-V_W, and ZnO/WSe_2-V_{Se}. Fermi levels are represented by dashed lines, and the CBM and VBM are marked by black stars.

At the same time, we compared the electron density difference before and after vacancy generation, as shown in Figure 6. Blue represents charge depletion and red represents charge accumulation. It can be seen from the figure that there is a certain rule of charge depletion and accumulation. There is charge depletion near Zn and W atoms and a large amount of charge accumulation around O and Se atoms. Among them, the charge distribution around each monolayer atom in ZnO/WSe_2 heterostructure is similar, and there are charge depletion and charge accumulation between monolayers. After the relaxation, due to the absence of a Zn atom, the not bound O atom moves to the WSe_2, resulting in a great change in the structure of the ZnO. At the same time, the charge accumulation around the O atom also leads to an increase in the charge depletion around the W atom. That may be the reason why the vacancy formation energy of ZnO/WSe_2-V_{Zn} is negative. However, the formation of the O, W, and Se vacancies has little effect on the structure of each monolayer, and the charge distribution is regular. Among them, the formation of the O vacancy has the least effect on the structure and charge distribution; After the Se vacancy is generated, the interlayer spacing between WSe_2-V_{Se} and ZnO is greatly reduced, the

charge accumulation and consumption between layers are increased, and the interlayer bonding is more stable, which is the same as the calculation results in Section 3.1. vacancies will change the electronic structure of ZnO/WSe_2 heterostructure and then affect the optical properties. Therefore, it is necessary to study the optical properties of ZnO/WSe_2 heterostructure.

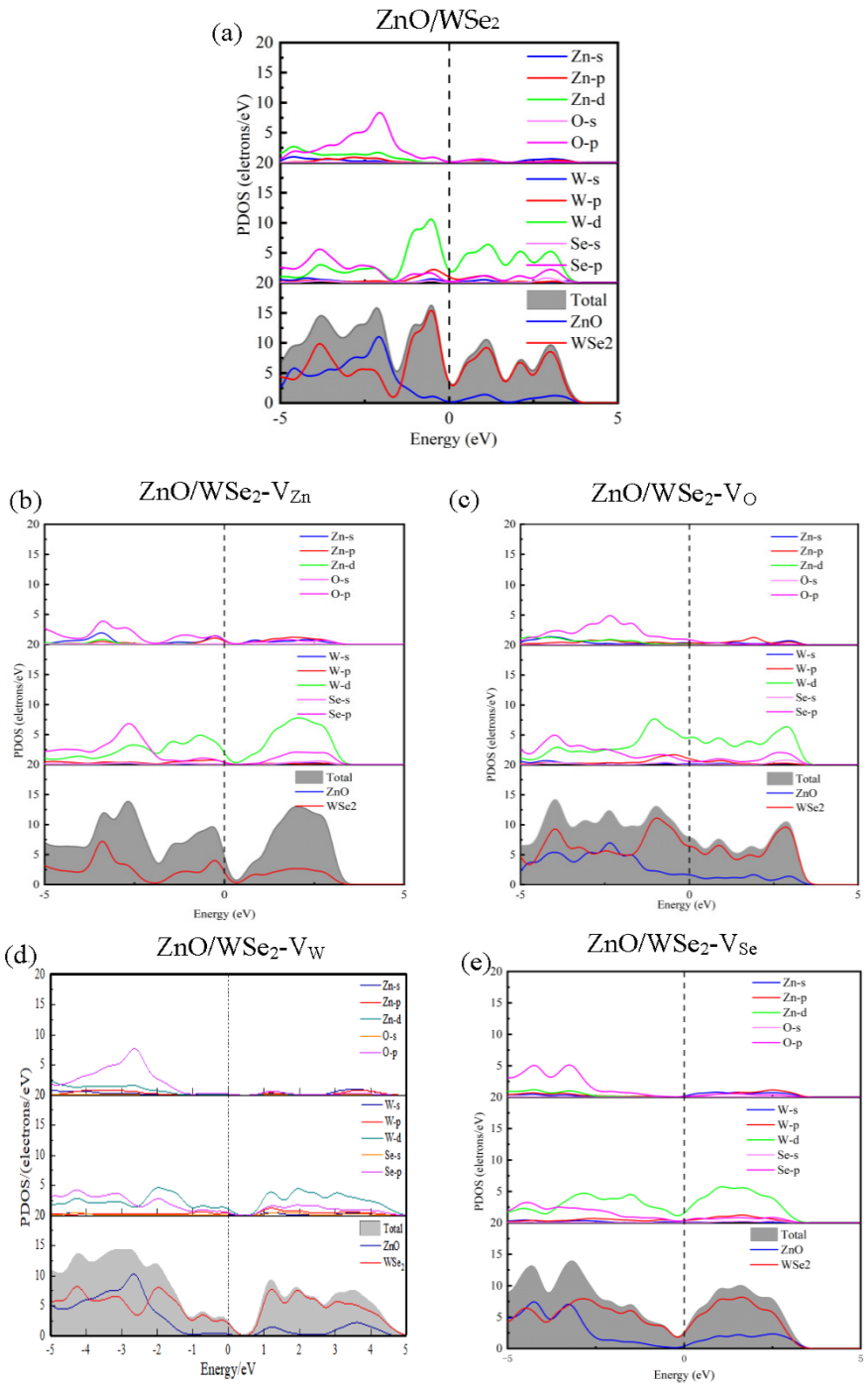

Figure 5. The partial density of states (PDOS) of ZnO/WSe_2 heterostructure, ZnO/WSe_2-V_{Zn}, ZnO/WSe_2-V_O, ZnO/WSe_2-V_W, and ZnO/WSe_2-V_{Se}. (**a**) ZnO/WSe_2 heterostructure; (**b**) ZnO/WSe_2-V_{Zn}; (**c**) ZnO/WSe_2-V_O; (**d**) ZnO/WSe_2-V_W; (**e**) ZnO/WSe_2-V_{Se}.

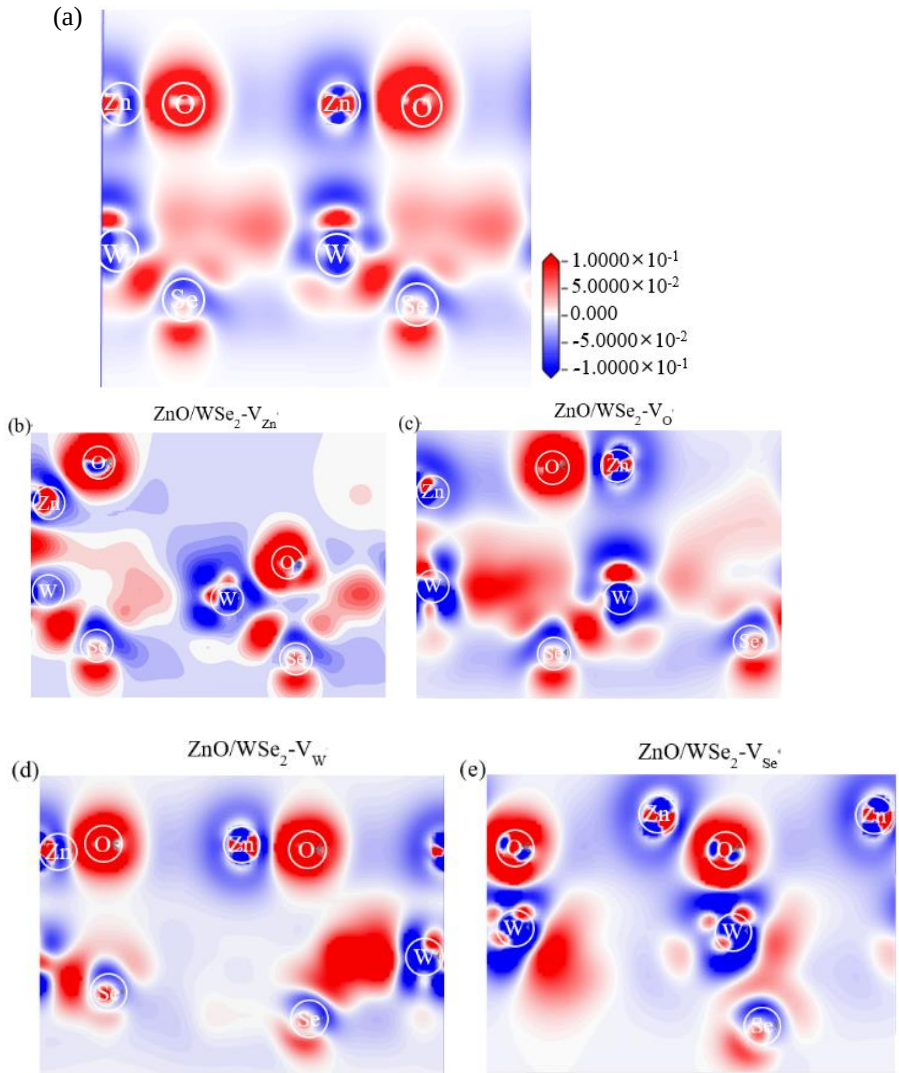

Figure 6. The electron differential density of after ZnO/WSe_2 heterostructure, ZnO/WSe_2-V_{Zn}, ZnO/WSe_2-V_O, ZnO/WSe_2-V_W, and ZnO/WSe_2-V_{Se}. The red represents charge accumulation and the blue represents charge depletion. (**a**) ZnO/WSe_2 heterostructure; (**b**) ZnO/WSe_2-V_{Zn} heterostructure; (**c**) ZnO/WSe_2-V_O heterostructure; (**d**) ZnO/WSe_2-V_W heterostructure; (**e**) ZnO/WSe_2-V_{Se} heterostructure.

3.3. Optical Properties

It is very necessary to study the optical properties of heterojunction, because optical properties play an important role in photoelectric detection equipment and electronic equipment [39,40]. It is proved that the heterojunction formed by coupling two different semiconductor materials will improve the optical properties of semiconductor materials [41,42]. Therefore, we studied and compared the optical properties of ZnO/WSe_2 heterostructures before and after vacancy generation, including dielectric function and optical absorption coefficient, as shown in Figure 7. According to Formula 3 in Section 2, the frequency dependent dielectric function shows how the incident light interacts when propagating in the material [43].The real part and imaginary part describe the dispersion and absorption effects respectively, i.e., $\varepsilon(\omega) = \varepsilon_1(\omega) + i\varepsilon_2(\omega)$ [44,45]. The imaginary part is related to the energy dissipation entering the medium, in other words, it is related to the photon absorption in the compound.

Figure 7a is the imaginary part of dielectric function. It can be seen from the figure that after the vacancy of ZnO/WSe_2 heterostructure is generated, the imaginary part of the dielectric function has changed greatly, especially in the infrared light region ($\lambda \geq 700$ nm).

When the vacancy of O and W is generated, the imaginary part of the dielectric function increases greatly, while the value of it decreases after Zn and Se vacancy is generated. Among them, ZnO/WSe_2-V_W heterostructure changes most obviously. According to the analysis in Figure 7b, the ZnO/WSe_2 heterostructure has absorption peaks in the ultraviolet region, visible region, and infrared region. When λ is about 500 nm, the optical absorption peaks of V_{Zn} and V_O are slightly larger than that of ZnO/WSe_2 heterostructure, indicating that the visible light absorption of heterostructure is enhanced after the formation of Zn and O vacancies; When $\lambda \geq 1000$ nm, the optical absorption coefficients of V_W and V_{Se} are larger than those of ZnO/WSe_2 heterostructure, which indicates that the absorption of infrared light is enhanced after the generation of W and Se vacancies. In conclusion, the optical properties of the ZnO/WSe_2 heterostructure will be changed due to the generation of vacancies. The generation of O and W vacancies is accompanied by an obvious red shift, and the generation of Zn and Se vacancies is accompanied by a blue shift. ZnO/WSe_2-V_{Zn}, ZnO/WSe_2-V_O heterostructures can be applied to the absorption and conversion of visible light and become an important photocatalyst; ZnO/WSe_2-V_O, ZnO/WSe_2-V_W heterostructures have good potential and wide application prospects in infrared light conversion, detection, and other aspects. At the same time, we should try to avoid the production of ZnO/WSe_2-V_{Se} heterostructure.

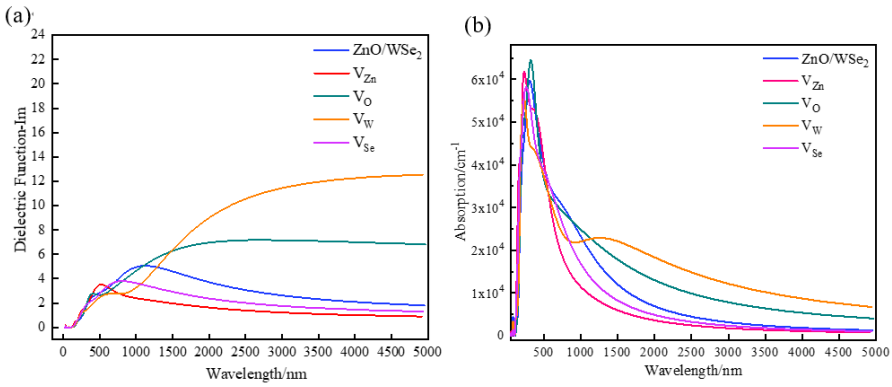

Figure 7. (**a**) The imaginary part of the dielectric function and (**b**) the light absorption coefficient of ZnO/WSe_2 heterostructure, ZnO/WSe_2-V_{Zn}, ZnO/WSe_2-V_O, ZnO/WSe_2-V_W, and ZnO/WSe_2-V_{Se}.

4. Conclusions

In this work, based on the first principles calculation of density functional theory (DFT), we studied the band structure changes of monolayer ZnO and WSe_2 before and after vacancy generation, and systematically studied the vacancy formation energy, band structure, density of states, electronic density difference and optical properties of ZnO/WSe_2 heterostructure before and after vacancy generation. The results show that the vacancy formation energy of Zn is negative and the others are positive; The band structure and bandgap of monolayer ZnO, WSe_2 and ZnO/WSe_2 heterostructure are changed due to the generation of vacancies. $ZnO-V_{Zn}$ and ZnO/WSe_2-V_O heterostructure show metallic properties; The generation of certain vacancies leads to the transition from direct bandgap semiconductor to indirect bandgap semiconductor. Through the analysis of the imaginary part of the dielectric function and optical absorption coefficient, the generation of vacancy will lead to the change of optical properties of the ZnO/WSe_2 heterostructure. The generation of O and W vacancies is accompanied by an obvious red shift, and the generation of Zn and Se vacancies is accompanied by blue shift. ZnO/WSe_2-V_{Zn}, ZnO/WSe_2-V_O heterostructures can be applied to the absorption and conversion of visible light and become an important photocatalyst; ZnO/WSe_2-V_O, ZnO/WSe_2-V_W heterostructures have good potential and wide application prospects in infrared light conversion, detection, and other aspects. In a word, the generation of vacancy changes the electrical and optical properties of ZnO/WSe_2 heterostructure, which provides a feasible strategy for adjusting

the photoelectric properties of two−dimensional photoelectric nano devices and has good potential and broad application prospects.

Author Contributions: Writing—original draft preparation, X.Y.; investigation, A.W.; writing—review and editing, L.D.; Conceptualization and software, X.Z.; methodology, J.L. All authors have read and agreed to the published version of the manuscript.

Funding: This research received no external funding.

Data Availability Statement: The data that support the findings of this study are available upon reasonable request from the authors.

Conflicts of Interest: The authors declare no conflict of interest.

References

1. Obeid, M.M.; Bafekry, A.; Rehman, S.U.; Nguyen, C.V. A type-II GaSe/HfS_2 van der Waals heterostructure as promising photocatalyst with high carrier mobility. *Appl. Surf. Sci.* **2020**, *534*, 147607. [CrossRef]
2. Wang, B.-J.; Li, X.-H.; Cai, X.-L.; Yu, W.-Y.; Zhang, L.-W.; Zhao, R.-Q.; Ke, S.-H. Blue phosphorus/Mg $(OH)_2$ van der Waals heterostructures as promising visible-light photocatalysts for water splitting. *J. Phys. Chem. C* **2018**, *122*, 7075–7080. [CrossRef]
3. Fujishima, A.; Honda, K. Electrochemical photolysis of water at a semiconductor electrode. *Nature* **1972**, *238*, 37–38. [CrossRef] [PubMed]
4. Nguyen, H.T.; Vu, T.V.; Binh, N.T.; Hoat, D.; Hieu, N.V.; Nguyen, C.V.; Phuc, H.V.; Jappor, H.R.; Obeid, M. Strain-tunable electronic and optical properties of monolayer GeSe: Promising for photocatalytic water splitting applications. *Chem. Phys.* **2020**, *529*, 110543. [CrossRef]
5. Neto, A.H.C.; Guinea, F.; Peres, N.M.R.; Novoselov, K.S.; Geim, A.K. The electronic properties of graphene. *Rev. Mod. Phys.* **2009**, *81*, 109. [CrossRef]
6. Novoselov, K.S.; Geim, A.K.; Morozov, S.V.; Jiang, D.; Zhang, Y.; Dubonos, S.V.; Grigorieva, I.V.; Firsov, A.A. Electric field effect in atomically thin carbon films. *Science* **2004**, *306*, 666–669. [CrossRef]
7. Novoselov, K.S.; Jiang, D.; Schedin, F.; Booth, T.J.; Khotkevich, V.V.; Morozov, S.V.; Geim, A.K. Two-dimensional atomic crystals. *Proc. Natl. Acad. Sci. USA* **2005**, *102*, 10451–10453. [CrossRef]
8. Wang, Q.H.; Kalantar-Zadeh, K.; Kis, A.; Coleman, J.N.; Strano, M.S. Electronics and optoelectronics of two-dimensional transition metal dichalcogenides. *Nat. Nanotechnol.* **2012**, *7*, 699–712. [CrossRef]
9. Ponce, F.A.; Bour, D.P. Nitride-based semiconductors for blue and green light-emitting devices. *Nature* **1997**, *386*, 351–359. [CrossRef]
10. Green, M.A.; Bremner, S.P. Energy conversion approaches and materials for high-efficiency photovoltaics. *Nat. Mater.* **2017**, *16*, 23–34. [CrossRef]
11. Polman, A.; Knight, M.; Garnett, E.C.; Ehrler, B.; Sinke, W.C. Photovoltaic materials: Present efficiencies and future challenges. *Science* **2016**, *352*, aad4424. [CrossRef]
12. Green, M.A.; Hishikawa, Y.; Warta, W.; Dunlop, E.D.; Levi, D.H.; Hohl-Ebinger, J.; Ho-Baillie, A.W.H. Solar cell efficiency tables (version 50). *Prog. Photovolt. Res. Appl.* **2017**, *25*, 668–676. [CrossRef]
13. Ohno, H.; Munekata, H.; Penney, T.; von Molnár, S.; Chang, L.L. Magnetotransport properties of p-type (In, Mn) As diluted magnetic III-V semiconductors. *Phys. Rev. Lett.* **1992**, *68*, 2664. [CrossRef]
14. Dietl, T.; Ohno, H. Dilute ferromagnetic semiconductors: Physics and spintronic structures. *Rev. Mod. Phys.* **2014**, *86*, 187. [CrossRef]
15. King, T.C.; Yang, Y.P.; Liou, Y.S.; Wu, C.J. Tunable defect mode in a semiconductor-dielectric photonic crystal containing extrinsic semiconductor defect. *Solid State Commun.* **2012**, *152*, 2189–2192. [CrossRef]
16. Mak, K.F.; Lee, C.; Hone, J.; Shan, J.; Heinz, T.F. Atomically thin MoS_2: A new direct-gap semiconductor. *Phys. Rev. Lett.* **2010**, *105*, 136805. [CrossRef]
17. Dolui, K.; Rungger, I.; Pemmaraju, C.D.; Sanvito, S. Possible doping strategies for MoS_2 monolayers: An ab initio study. *Phys. Rev. B* **2013**, *88*, 075420. [CrossRef]
18. Komsa, H.-P.; Kotakoski, J.; Kurasch, S.; Lehtinen, O.; Kaiser, U.; Krasheninnikov, A. Two-dimensional transition metal dichalcogenides under electron irradiation: Defect production and doping. *Phys. Rev. Lett.* **2012**, *109*, 035503. [CrossRef]
19. Segovia-Chaves, F.; Vinck-Posada, H. Effects of hydrostatic pressure on the band structure in two-dimensional semiconductor square photonic lattice with defect. *Phys. B Condens. Matter* **2018**, *545*, 203–209. [CrossRef]
20. Zak, A.; Feldman, Y.; Lyakhovitskaya, V.; Leitus, G.; Popovitz-Biro, R.; Wachtel, E.; Cohen, H.; Reich, S.; Tenne, R. Alkali metal intercalated fullerene-like MS_2 (M = W.; Mo) nanoparticles and their properties. *J. Am. Chem. Soc.* **2002**, *124*, 4747–4758. [CrossRef]
21. Kabita, K.; Maibam, J.; Sharma, B.I.; Thapa, R.K.; Brojen Singh, R.K. First principle study on pressure-induced electronic structure and elastic properties of indium phosphide (InP). *Indian J. Phys.* **2015**, *89*, 1265–1271. [CrossRef]
22. Mellot-Draznieks, C. Role of computer simulations in structure prediction and structure determination: From molecular compounds to hybrid frameworks. *J. Mater. Chem.* **2007**, *17*, 4348–4358. [CrossRef]

23. Lejaeghere, K.; Bihlmayer, G.; Björkman, T.; Blaha, P.; Blügel, S.; Blum, V.; Caliste, D.; Castelli, I.E.; Clark, S.J.; Corso, A.D.; et al. Reproducibility in density functional theory calculations of solids. *Science* **2016**, *351*, aad3000. [CrossRef] [PubMed]
24. Kohn, W.; Sham, L.J. Self-consistent equations including exchange and correlation effects. *Phys. Rev.* **1965**, *140*, A1133. [CrossRef]
25. Segall, M.D.; Lindan, P.J.D.; Probert, M.J.; Pickard, C.J.; Hasnip, P.J.; Clark, S.J.; Payne, M.C. First-principles simulation: Ideas, illustrations and the CASTEP code. *J. Phys. Condens. Matter* **2002**, *14*, 2717. [CrossRef]
26. Perdew, J.P.; Burke, K.; Ernzerhof, M. Generalized gradient approximation made simple. *Phys. Rev. Lett.* **1996**, *77*, 3865. [CrossRef]
27. Heyd, J.; Scuseria, G.E.; Ernzerhof, M. Hybrid functionals based on a screened Coulomb potential. *J. Chem. Phys.* **2003**, *118*, 8207–8215. [CrossRef]
28. Hu, F.; Tao, L.; Ye, H.; Li, X.; Chen, X. ZnO/WSe_2 vdW heterostructure for photocatalytic water splitting. *J. Mater. Chem. C* **2019**, *7*, 7104–7113. [CrossRef]
29. Zheng, H.; Li, X.-B.; Chen, N.-K.; Xie, S.-Y.; Tian, W.Q.; Chen, Y.; Xia, H.; Zhang, S.B.; Sun, H.-B. Monolayer II-VI semiconductors: A first-principles prediction. *Phys. Rev. B* **2015**, *92*, 115307. [CrossRef]
30. Perdew, J.P.; Burke, K.; Ernzerhof, M. *Local and Gradient-Corrected Density Functionals, Chemical Applications of Density-Functional Theory*; Laird, B.B., Ross, R.B., Ziegler, T., Eds.; American Chemical Society: Washington, DC, USA, 1996; pp. 453–462.
31. Zhang, Y.; Yang, W. Comment on "Generalized gradient approximation made simple". *Phys. Rev. Lett.* **1998**, *80*, 890. [CrossRef]
32. Wu, Z.; Cohen, R.E. More accurate generalized gradient approximation for solids. *Phys. Rev. B* **2006**, *73*, 235116. [CrossRef]
33. Friák, M.; Šob, M.; Vitek, V. Ab initio study of the ideal tensile strength and mechanical stability of transition-metal disilicides. *Phys. Rev. B* **2003**, *68*, 184101. [CrossRef]
34. Lee, H.-S.; Mizoguchi, T.; Yamamoto, T.; Kang, S.L.; Ikuharaa, Y. First-principles calculation of defect energetics in cubic-$BaTiO_3$ and a comparison with $SrTiO_3$. *Acta Mater.* **2007**, *55*, 6535–6540. [CrossRef]
35. Ge, F.F.; Wu, W.D.; Cao, L.H.; Wang, X.M.; Wang, H.P.; Dai, Y.; Wang, H.B.; Shen, J. The structure and defect formation energy in tetragonal $PbTiO_3$: Ab initio calculation. *Ferroelectrics* **2010**, *401*, 154–160. [CrossRef]
36. Shang, J.; Pan, L.; Wang, X.; Li, J.; Deng, H.-X.; Wei, Z. Tunable electronic and optical properties of InSe/InTe van der Waals heterostructures toward optoelectronic applications. *J. Mater. Chem. C* **2018**, *6*, 7201–7206. [CrossRef]
37. Sun, S.; Meng, F.; Wang, H.; Wang, H.; Ni, Y. Novel two-dimensional semiconductor SnP_3: High stability, tunable bandgaps and high carrier mobility explored using first-principles calculations. *J. Mater. Chem. A* **2018**, *6*, 11890–11897. [CrossRef]
38. Yu, H.B.; Wang, W.H.; Bai, H.Y. An electronic structure perspective on glass-forming ability in metallic glasses. *Appl. Phys. Lett.* **2010**, *96*, 081902.
39. Zhang, C.; Zhou, Y.; Zhang, Y.; Zhao, S.; Fang, J.; Sheng, X.; Zhang, H. Self-assembly hierarchical silica nanotubes with vertically aligned silica nanorods and embedded platinum nanoparticles. *ACS Sustain. Chem. Eng.* **2017**, *5*, 1578–1585. [CrossRef]
40. Grätzel, M. Photoelectrochemical Cells. In *Materials for Sustainable Energy: A Collection of Peer-Reviewed Research and Review Articles from Nature Publishing Group*; Nature: London, UK, 2011; pp. 26–32.
41. Zhu, L.; Cao, X.; Gong, C.; Jiang, A.; Cheng, Y.; Xiao, J. Preparation of Cu_3N/MoS_2 heterojunction through magnetron sputtering and investigation of its structure and optical performance. *Materials* **2020**, *13*, 1873. [CrossRef]
42. Hassan, M.A.; Kang, J.H.; Johar, M.A.; Ha, J.-S.; Ryu, S.-W. High-performance ZnS/GaN heterostructure photoanode for photoelectrochemical water splitting applications. *Acta Mater.* **2018**, *146*, 171–175. [CrossRef]
43. Djurišić, A.B.; Li, E.H. The Optical Dielectric Function: Excitonic Effects at E_0 Critical Point. *J. Phys. Soc. Jpn.* **2001**, *70*, 2164–2167. [CrossRef]
44. Fadaie, M.; Shahtahmassebi, N.; Roknabad, M.R. Effect of external electric field on the electronic structure and optical properties of stanene. *Opt. Quantum Electron.* **2016**, *48*, 1–12. [CrossRef]
45. Sun, M.; Chou, J.-P.; Gao, J.; Cheng, Y.; Hu, A.; Tang, W.; Zhang, G. Exceptional optical absorption of buckled arsenene covering a broad spectral range by molecular doping. *ACS Omega* **2018**, *3*, 8514–8520. [CrossRef] [PubMed]